Inorganic Chemistry

Article

pubs.acs.org/IC

# Rapid Hydrothermal Synthesis of $VO_2$ (B) and Its Conversion to Thermochromic $VO_2$ (M1)

Srinivasa Rao Popuri,[†,‡,§] Marinela Miclau,[§] Alla Artemenko,[†,‡] Christine Labrugere,[∥] Antoine Villesuzanne,[†,‡] and Michaël Pollet*[,†,‡]

[†]Institut de Chimie de la Matière Condensée de Bordeaux (ICMCB), Centre National de la Recherche Scientifique (CNRS), UPR 9048, F-33600 Pessac, France

[‡]Institut de Chimie de la Matière Condensée de Bordeaux, Université de Bordeaux (ICMCB), UPR 9048, F-33600 Pessac, France

[§]Institutul National de Cercetare—Dezvoltare Pentru Electrochimie si Materie Condensata (INCEMC), Plautius Andronescu 1, 300224 Timisoara, Romania

[∥]Centre de Caractérisation des Matériaux Avancés (CeCaMA), Institut de Chimie de la Matière Condensée de Bordeaux (ICMCB), UPR 9048, F-33600 Pessac, France

**ABSTRACT:** The present study provides a rapid way to obtain $VO_2$ (B) under economical and environmentally friendly conditions. $VO_2$ (B) is one of the well-known polymorphs of vanadium dioxide and is a promising cathode material for aqueous lithium ion batteries. $VO_2$ (B) was successfully synthesized by rapid single-step hydrothermal process using $V_2O_5$ and citric acid as precursors. The present study shows that phase-pure $VO_2$ (B) polytype can be easily obtained at 180 °C for 2 h and 220 °C for 1 h, that is, the lowest combination of temperature and duration reported so far. The obtained $VO_2$ (B) is characterized by X-ray powder diffraction, high-resolution scanning electron microscopy, and Fourier transform infrared spectroscopy. In addition, we present an indirect way to obtain $VO_2$ (M1) by annealing $VO_2$ (B) under vacuum for 1 h.

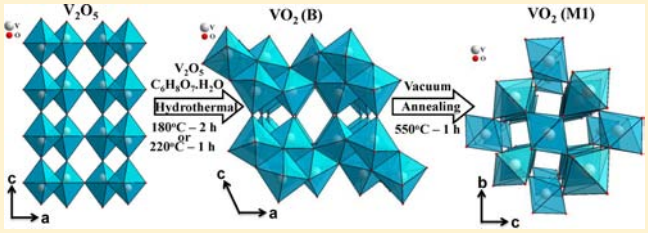


## 1. INTRODUCTION

Among the transition metal oxides, vanadium-based oxides are receiving a tremendous attention because of their diverse chemical structures, novel properties, abundance in nature, and potential applications. Beyond well-known oxides $V_2O_3$, $VO_2$, and $V_2O_5$, with oxidation states from 3+ to 5+, the richness of the V−O system stands both in its very rich solid state phase diagram, due to presence of several Magneli and Wadsley phases, and its hydrothermal phase diagram with several metastable, stable hydrate, and nonhydrate phases.[1,2] Such richness and complexity of the phase diagrams generally makes formation and stabilization of each specific phase very challenging. Till now, several kinds of crystalline phases of V−O and V−H−O systems have been reported, including rutile $VO_2$ (R),[3] monoclinic $VO_2$ (M1),[4] monoclinic $VO_2$ (M2),[5] tetragonal $VO_2$ (A),[6] monoclinic $VO_2$ (B),[7] $VO_2$ (D),[8] BCC $VO_2$,[9] paramontroseite $VO_2$,[10] orthorhombic $VO_2{\cdot}H_2O$ or $VO_2$ (C),[11] $V_2O_4{\cdot}2H_2O$,[12] $V_{10}O_{24}{\cdot}9H_2O$,[13] $V_3O_7{\cdot}H_2O$,[14] haggite $H_4V_4O_{10}$,[15] and montroseite VOOH.[16] Out of these phases, $VO_2$ (M1) has been attracting much attention due to its unique near room temperature insulator-to-metal phase transition and technological applicability. Beyond $VO_2$ (M1), recently $VO_2$ (B) is of great interest owing to its layered structure, high energy capacity along with moderate work potential, and promising applications in the field of energy technologies.[17−19] Through preparing nanotextured $VO_2$ (B) cathode material from vanadium oxide aerogels, very high specific capacity of 500 mA·h/g was reported by Baudrin et al.[20] In the case of nanostructures, initial high capacity was ascribed to the large surface area and short diffusion distances.[21] The operating properties of battery materials depend not only on the structure but also on the morphology of the electrode component. Based on this, in recent years some efforts have been devoted to the elaboration of 1D nanostructured $VO_2$ (B) materials (i.e., nanorods, nanowires, nanoribbons, nanospheres, and nanobelts) and to the improvement of their electrochemical performance.[22−26] Until now, two main different preparation techniques were used to obtain $VO_2$ (B): a hydrothermal method or reduction of vanadium oxide precursors under different atmospheres. Among these, hydrothermal methods provide numerous advantages by offering several variable preparation parameters: time, temperature, pH, concentration, filling percentage of the autoclave, precursor dependence, pressure, reducing agents, etc. These parameters are often very useful to obtain desired morphologies and explore new phases. For example, pH-dependent morphologies and pressure-dependent phase formation were reported in the case of $VO_2$ polymorhs.[26,27] From an economical and environmental point of view, however, it is necessary to

**Received:** June 6, 2012
**Published:** April 12, 2013

   dx.doi.org/10.1021/ic301201k | *Inorg. Chem.* 2013, 52, 4780−4785

synthesize $VO_2$ nanostructures at low temperature and duration using abundant, inexpensive, and nontoxic precursors. In this study, we propose a rapid hydrothermal synthesis of $VO_2$ (B) platelet morphologies using a novel combination of precursors, together with low synthesis temperature and duration. This hydrothermal synthesis protocol allowed us also to propose a fast synthesis method for the thermochromic $VO_2$ (M1) polymorph.

## 2. EXPERIMENTAL SECTION

**2.1. Synthesis.** All chemical reagents were analytical grade and used as received without any further purification. The samples were synthesized via a rapid hydrothermal process as follows. Vanadium pentaoxide ($V_2O_5$, 2.6 mmol; Aldrich) was dissolved in 43 mL of deionized water. After stirring for 15 min using a magnetic stirrer, 3.9 mmol of citric acid monohydrate ($C_6H_8O_7{\cdot}H_2O$; Merck) was added into the solution and stirring was prolonged for 15 min. The resultant yellow aqueous solution was transferred into the Teflon liner of a stainless steel autoclave. The sealed steel autoclave was kept in an oven at 120−220 °C for 0.5−12 h. After the reaction process, the autoclave was slowly cooled to room temperature. The as-prepared powder samples were filtered and washed with distilled water and ethanol to remove unreacted chemical species and dried in air at 80 °C for 6 h. The final obtained blue powders were used for further characterization.

**2.2. Characterization.** The purity of as-synthesized powders was checked by X-ray powder diffraction (XRPD; PANalytical X'Pert PRO MPD diffractometer) using Cu K$\alpha$ radiation at 40 keV and 30 mA, with divergent slit of 1° and receiving slit size of 0.1 mm in a 2$\theta$ range between 10° and 100° with a 0.01313° step size and 700 s count time per step. The identification of the compound was made by comparing the experimental XPRD patterns to standards compiled by the Joint Committee on Powder Diffraction and Standards (JCPDS data card 01-081-2392). The morphology and microstructure of the synthesized compounds were investigated by high-resolution scanning electron microscopy (HRSEM; JSM 6700F) under 5 keV: the powder samples were deposited and adhered to carbon tapes and subsequently sputter-coated with a thin layer of gold on the surface to prevent charging effects. A Fourier transform infrared spectrometer (FTIR-8400S, Shimadzu) was used to confirm the formation and purity of the desired compound; spectra were acquired on mixtures of $VO_2$ (B) and KBr in the wavenumber range 400−2800 $cm^{-1}$ and averaged over 100 scans. The above-mentioned XRPD diffractometer was further used with a high-temperature chamber under vacuum ($9.2 \times 10^{-5}$ bar) to study the phase transition between two different polytypes of vanadium dioxide; the powder of $VO_2$ (B) was dispersed in ethanol and then deposited on the platinum strip of an Anton Paar high-temperature chamber; the diffractometer was calibrated using the peak shift of the platinum strip; the HT-XRPD patterns were acquired using 0.003° step and 66 s count time per step, under $9.2 \times 10^{-5}$ bar.

## 3. RESULTS AND DISCUSSION

To present the structural relationship between $VO_2$ (B) and $VO_2$ (M1), in comparison with $V_2O_5$, the crystal structures of orthorhombic $V_2O_5$, monoclinic $VO_2$ (B), and monoclinic $VO_2$ (M1) are shown in Figure 1. $V_2O_5$ consists of layers of edge- and corner-sharing octahedra along the *ab* planes. These layers are connected at corners to give a three-dimensional lattice pattern. $VO_2$ (B) exhibits two edge-sharing units to produce a layer of octahedra along the *ab* plane. These layers are connected by corners to give a three-dimensional crystal structure. In this case, the 4-fold axes of oxygen octahedra are aligned along one direction only. The main difference between these two structures is that $VO_2$ (B) consists of two edge-sharing octahedra units, instead of one edge-shared and one corner-shared as in case of $V_2O_5$. On the other hand, the difference between $VO_2$ (B) and $VO_2$ (M1) is only the orientation of the 4-fold axis of oxygen octahedra. In the case of $VO_2$ (M1), the 4-fold axis of the oxygen octahedra is aligned along two perpendicular directions.

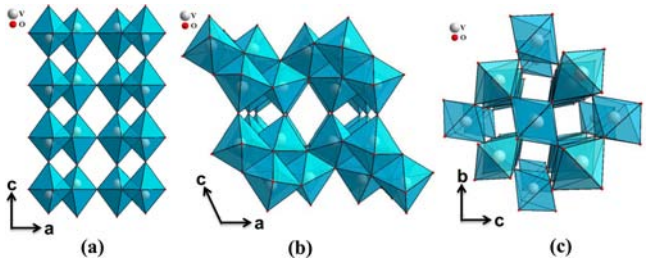


**Figure 1.** Crystal structures of (a) orthorhombic $V_2O_5$, (b) monoclinic $VO_2$ (B), and (c) monoclinic $VO_2$ (M1).

The complex aqueous chemistry of vanadium ($V^{5+}$) has been extensively studied for the past few decades. In aqueous solution and at room temperature, depending on concentration and pH, vanadium ions exist in at least 11 varieties of molecular hydrate species. Recently, using peroxovanadic acid and oxalic acid as precursors, Li et al. have obtained $VO_2$ (B) urchin-like nanostructures at 180 °C for 12 h.[28] This corresponds to the lowest optimized preparation conditions presented for $VO_2$ (B) so far. They have observed a transition from bariandite-type mineral $V_{10}O_{24}{\cdot}9H_2O$ to $VO_2$ (B) by a reduction−dehydration process. To optimize the synthesis conditions for $VO_2$ (B) and to study the evolution of phases as a function of temperature ($T$) and reaction time ($t$) at fixed concentration ($V_2O_5$ and citric acid), several experiments were made with $T$ =120, 150, 180, or 220 °C and $t$ = 0.5, 2, 3, 3.5, 6, 7.5, or 12 h. At 120 °C for 12 h, 150 °C for 2 h, 180 °C for 1 h, and 220 °C for 0.5 h reaction time, $VO_2{\cdot}xH_2O$ is systematically obtained (JCPDS data card 00-018-1445); below these preparation conditions, we observed bariandite-type mineral $V_{10}O_{24}{\cdot}9H_2O$ (JCPDS data card 00-025-1006).[29] When both reaction temperature and duration are further increased to 180 °C for 2, 6, or 12 h and 220 °C for 3, 3.5, or 7.5 h, $VO_2$ (B) polymorph forms. Figure 2

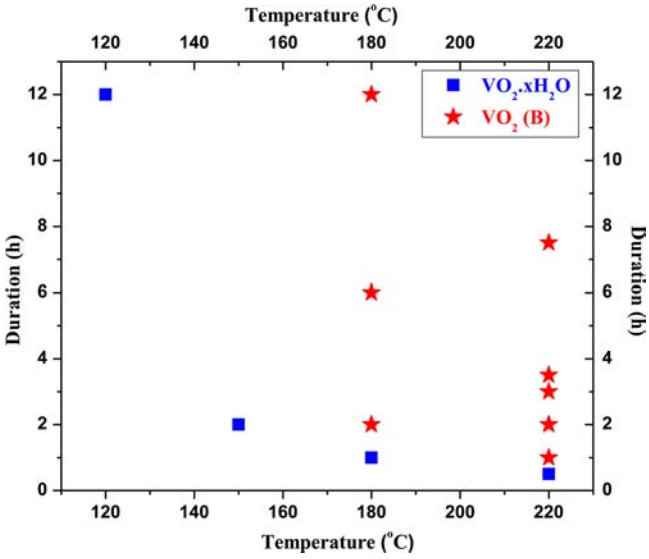


**Figure 2.** Kinetic phase evolution study between 120 and 220 °C in the duration range 0.5−12 h. $V_2O_5$ and citric acid were used as precursors under hydrothermal conditions. Squares represent $VO_2$ (B) phase, and stars represent the $VO_2{\cdot}xH_2O$ phase against the specified temperature and duration.


dx.doi.org/10.1021/ic301201k | Inorg. Chem. 2013, 52, 4780−4785

summarizes the evolution of phases with the temperature ($T$) and duration of reaction ($t$); it illustrates the $T-t$ exponential dependence for the formation of the hydrate (the necessary dwell time drops rapidly as the temperature increases) and demonstrates the stability of the B polytype at high temperature ($T \geq 180$ °C); it also gives insight to the phase-forming sequence, which is quite different from the mechanism observed in case of $VO_2$ (B) preparation under reducing atmospheres, with the formation of the intermediate compound $VO_2{\cdot}xH_2O$ between $V_{10}O_{24}{\cdot}9H_2O$ and $VO_2$ (B). The reducing mechanism from $V^{5+}$ ($V_2O_5$) to $V^{4+}$ ($VO_2$ (B)) in the presence of a reducing agent (citric acid) can actually be described with a three-step process from partial reduction−hydration to complete reduction−hydration and finally dehydration:

$$V_2O_5 + H_2O \rightarrow V_{10}O_{24}{\cdot}9H_2O$$

$$V_{10}O_{24}{\cdot}9H_2O + H_2O \rightarrow VO_2{\cdot}xH_2O$$

$$VO_2{\cdot}xH_2O + H_2O \rightarrow VO_2\ (B)$$

Here $V_{10}O_{24}{\cdot}9H_2O$ forms in the early stage of the reaction process under (soft-) reducing conditions or at low temperature; it is a layered compound, as expected from the ability of $V_2O_5$ to intercalate water in its layered structure. As the reduction reaction progresses, the remaining $V^{5+}$ ions are reduced to $V^{4+}$, resulting in $VO_2{\cdot}xH_2O$. In the final stage of reaction process, the dehydration of $VO_2{\cdot}xH_2O$ gives rise to the fully reduced $V^{4+}O_2$ (B).

Figure 3 shows the XRPD pattern of $VO_2$ (B) prepared at 220 °C for 2 h and refined using the FullProf program.[30] We

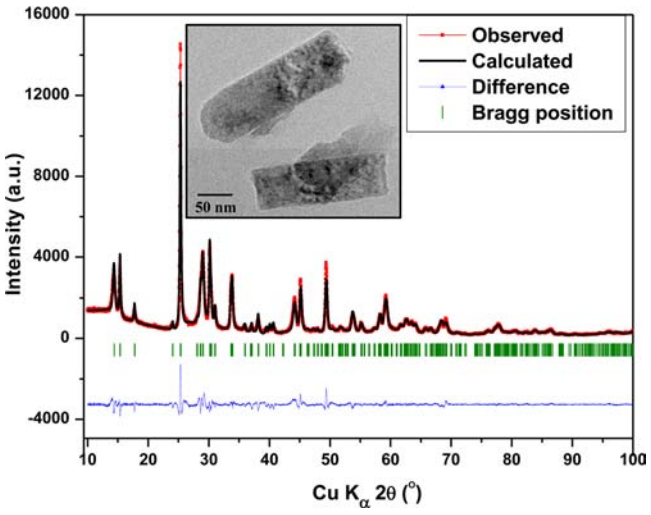


**Figure 3.** XRPD pattern of $VO_2$ (B) synthesized at 220 °C for 2 h (inset, platelet-like morphology of the $VO_2$ (B) crystals obtained using TEM).

used Thompson−Cox−Hastings pseudo-Voigt axial divergence asymmetry profile function for profile fitting. All diffraction peaks were indexed according to the monoclinic phase of $VO_2$ (B) with space group $C2/m$, lattice parameters $a$ = 12.0417(3) Å, $b$ = 3.6892(8) Å, $c$ = 6.4312(2) Å, and $\beta$ = 106.965(2)°; these results match with JCPDS data card 01-081-2392. The results from the Rietveld refinement are given in Table 1, and only a weak preferential orientation indicative of a platy habit was noticed. No trace of other phases or impurities was detected, independent of the present temperature and duration conditions, supporting the purity of the $VO_2$ (B) platelets. We

**Table 1. Lattice Parameters and Atomic Positions of $VO_2$ (B)**

| lattice parameters | profile parameters | | |
|---|---|---|---|
| space group, $C2/m$ (No. 12) | function | Thompson−Cox−Hastings pseudo-Voigt axial divergence asymmetry | |
| $a$ = 12.0417(3) Å | | | |
| $b$ = 3.6892(8) Å | half-width parameters | $U$ = 0.83(4) | |
| $c$ = 6.4312(2) Å | | $V$ = −0.35(3) | |
| $\beta$ = 106.965(2)° | | $W$ = 0.048(4) | |
| | atomic positions | | |
| atom label | Wyckoff position | $x$ | $z$ |
| V1 | 4i | 0.3003(2) | 0.7150(4) |
| V2 | 4i | 0.4005(2) | 0.3104(4) |
| O1 | 4i | 0.3591(5) | 0.987(1) |
| O2 | 4i | 0.2281(8) | 0.316(1) |
| O3 | 4i | 0.4534(8) | 0.677(2) |
| O4 | 4i | 0.1327(6) | 0.709(1) |
| reliability factors | $R_p$, 6.11% | $R_{wp}$, 7.92% | $\chi^2$, 3.97 |

calculated the average coherence length ($D$) by using the Scherrer expression, which is ca. 65 nm. The size and platelet-like morphology are consistent with TEM observations shown in the inset of Figure 3. The broadening of ($00l$) peaks compared with other reflections was already explained by disorientation in ($00l$) layers.[31] The platelet-like morphology of $VO_2$ (B) at different temperatures and durations is shown in Figure 4a−c The morphology of platelets is similar in all cases, which indicates that temperature and duration have minor effect on the morphology.

To investigate the chemical bonding between vanadium and oxygen ions and to confirm the phase purity, we performed FTIR spectroscopy. Figure 4d shows the FTIR spectrum of $VO_2$ (B) sample prepared at 220 °C for 2 h. The main vibrational bands observed from the FTIR spectrum are at 551, 669, 936, 1012, 1624, 2339, and 2360 $cm^{-1}$ and can be attributed to the various vibrational bands of V−O, O−H, and C−O systems. From the comparison with the spectra of pure KBr, only bands at 551, 936, and 1012 $cm^{-1}$ can be considered as intrinsic to vanadium oxide, which matches well with earlier reports: the initial broad vibrational band at 551 $cm^{-1}$ is assigned to the V−O−V octahedral bending modes;[31] the band at 936 $cm^{-1}$ is attributed to the coupled vibration of V═O and V−O−V;[32] the band at 1012 $cm^{-1}$ can attributed to the stretching of short V−O bonds that are also present in this phase. The high- and low-frequency bands arise from $CO_2$ as confirmed by electron spin resonance with a broad resonance in low magnetic field characteristic of surface adsorption of carboxyl and X-ray photoemission spectroscopy measurements at C 1s edge with the presence of a weak signal only on the uncleaved surface (not shown); such surface pollution of the powder sample can easily be due to the atmosphere exposure or partial interaction with the reducing agent during the synthesis. The asymmetrical stretch of $CO_2$ can give a strong band in the IR spectrum at 2350 $cm^{-1}$, and the bands appearing around this region (i.e., 2339, 2360 $cm^{-1}$) can be reasonably assigned to the asymmetrical stretch of $CO_2$ molecules; in the same way, the vibrational band appearing in at 666 $cm^{-1}$ can be assigned to degenerate bending vibration of $CO_2$. The band at 1624 $cm^{-1}$ can be assigned to different vibration models of an O−H group of adsorbed water molecules on the surface of the platelets.[33]


dx.doi.org/10.1021/ic301201k | Inorg. Chem. 2013, 52, 4780−4785

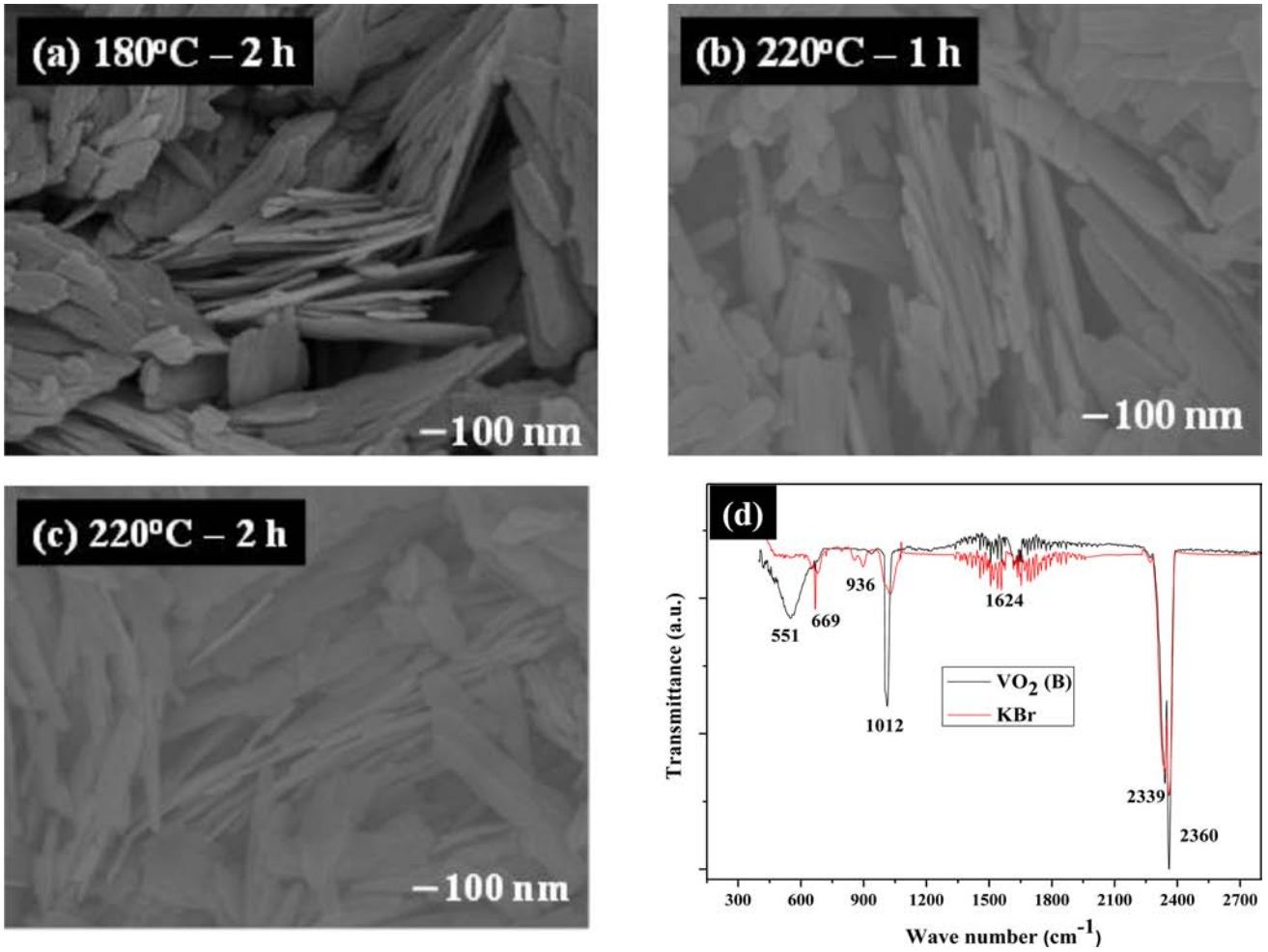


**Figure 4.** HRSEM images of $VO_2$ (B) synthesized at (a) 180 °C for 2 h, (b) 220 °C for 1 h, and (c) 220 °C for 2 h. (d) FT-IR spectra of $VO_2$ (B) sample prepared at 220 °C for 2 h.

These FT-IR observations confirm that the nanoplatelets correspond to the $VO_2$ phase.

The stability of $VO_2$ (B) was studied by high-temperature XRPD (HT-XRPD) under vacuum and differential scanning calorimetry (DSC) under 5 N argon flow (heating/cooling rate of 5 K/min). The use of either argon or vacuum is justified by the instability of $VO_2$ under oxidizing conditions. Indeed, Pavasupree et al. studied the stability of $VO_2$ (B) in air and observed that around 400 °C this polymorph was oxidized into $V_2O_5$ crystallized phase.[34] *In situ* HT-XRPD measurements (Figure 5a) show that $VO_2$ (B) is stable under vacuum up to 400 °C and that the transformation into $VO_2$ (M1) occurs only above 400 °C. At 500 °C, both B and M1 polymorphs coexist, and $VO_2$ (B) completely transforms into $VO_2$ (M1) around 600 °C. XRPD patterns at 200 and 25 °C recorded during the cooling process, with the presence of $VO_2$ (M1) phase only, support the irreversibility of the phase transformation. DSC measurements (Figure 5b) were carried out on $VO_2$ (B) powder samples. A first experiment up to 600 °C highlighted several transitions: a first one during the heating treatment beginning at ca. 350 °C and finishing at ca. 430 °C, immediately followed by a second broad one beginning at ca. 450 °C and continuing during the cooling stage, and a small last one during cooling coinciding with the transformation from $VO_2$ (R) into $VO_2$ (M1) (61.5 °C); the final compound after the DSC measurement can be refined with $VO_2$ (M1) space group and parameters. A second DSC experiment up to 430 °C only revealed the only presence of the first transition without any trace on cooling of the transformation from $VO_2$ (R) into $VO_2$ (M1); the final compound can here also be refined with $VO_2$ (M1) space group and parameters. A last experiment up to 150 °C carried out on the latter sample evidenced on both heating and cooling the reversible transition from $VO_2$ (M1) into $VO_2$ (R) at 69.5 and 65.2 °C, respectively (confirmed by magnetization measurements, *not shown*); as previously, the final compound can again be refined with $VO_2$ (M1) space group and parameters. The transition on heating in the temperature range 350–430 °C can be interpreted as the nonreversible transformation from $VO_2$ (B) into $VO_2$ (M1); the temperature for the transformation using argon flow is slightly lower than in the case of the use of vacuum. The second transition at high temperature may be related to a partial transformation to $VO_2$ (R) giving rise to the peak observed at 61.5 °C during the first experiment. Both the *in situ* HT-XRPD and DSC measurements show that $VO_2$ (B) actually transforms into $VO_2$ (M1) at high temperature. Indeed, both the XRD and the third DSC experiments show that the product after the second DSC experiment is $VO_2$ (M1); however, no transition from R to M1 could be detected from the second DSC experiment evidencing that the structure evolve from $VO_2$ (B) to $VO_2$ (M1) despite the transformation occurs at high temperature. None of our experiments could reveal the


dx.doi.org/10.1021/ic301201k | *Inorg. Chem.* 2013, 52, 4780–4785

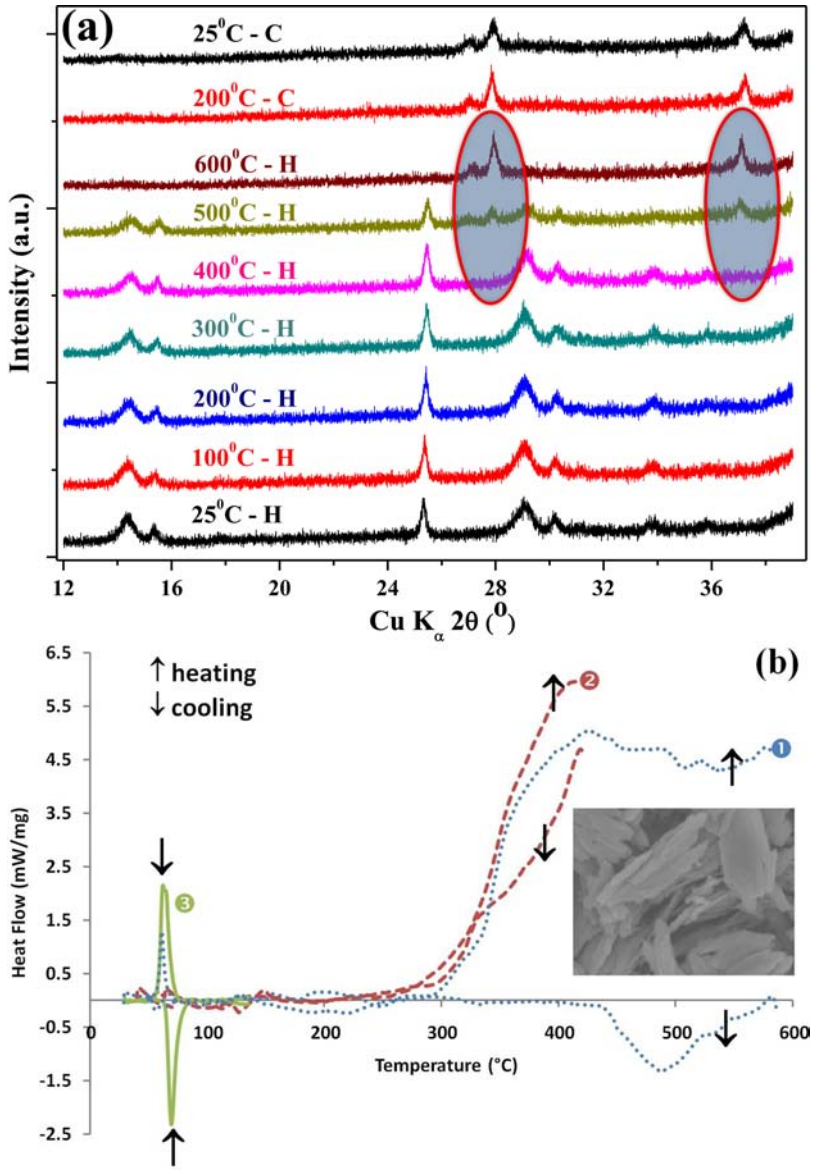


**Figure 5.** (a) Phase transformation study of $VO_2$ (B) into $VO_2$ (M1) by *in situ* HT-XRPD from 25 to 600 °C (heating cycle (H)) and 600 to 25 °C (cooling cycle (C)). The circles highlight the transformation into $VO_2$ (M1). (b) Phase transition study of $VO_2$ (B) into $VO_2$ (M1) by DSC under argon flow: (1) DSC experiment up to 600 °C, (2) DSC experiment up to 430 °C, and (3) DSC experiment up to 150 °C on the sample produced by treatment 2. The inset shows the morphology after annealing at 550 °C for 1 h.

presence of any intermediate phase; however, we could observe that an increase in the temperature could promote the transformation of $VO_2$ (M1) into $VO_2$ (R) evidenced along with a small peak at 61.5 °C. Our observations are consistent with previous reports, which showed that platelet $VO_2$ (B) powders were transformed into $VO_2$ (M1) using either *in situ* electron microscopy study[35] or the temperature evolution of FTIR spectra.[31] Finally to prepare thermochromic $VO_2$ (M1), we annealed $VO_2$ (B) samples for 1 h at 550 °C in vacuum-sealed silica tubes (2 and 5 °C/min heating and cooling rates respectively). The XRPD study at room temperature demonstrated the formation of $VO_2$ (M1), and the inset of Figure 5b shows the SEM image of $VO_2$ (M1) obtained after annealing treatment at 550 °C for 1 h. The retention of platelet morphology indicates the minor influence of the thermal treatment. This process can be used as a rapid indirect way (total 2 h) to prepare the $VO_2$ (M1) polymorph; usually, several days are required for obtaining the pure phase.

## 4. CONCLUSION

We proposed a convenient, rapid hydrothermal synthesis of vanadium dioxide B polymorph. We used an environmentally friendly novel combination of precursors $V_2O_5$ and citric acid to obtain $VO_2$ (B) platelets. Phase purity and formation process were confirmed using X-ray powder diffraction and Fourier transform infrared spectroscopy, respectively. $VO_2$ (B) phase transition studies under vacuum demonstrate a one-step transformation into $VO_2$ (M1) that allows us to present an indirect rapid preparation method for $VO_2$ (M1). The versatility of this method can be extended to the preparation of other transition metal oxides.


dx.doi.org/10.1021/ic301201k | *Inorg. Chem.* 2013, 52, 4780−4785

## AUTHOR INFORMATION


### Corresponding Author

*Mailing address: ICMCB-CNRS, 87 avenue du Dr Albert Schweitzer, 33608 Pessac Cedex, France. E-mail: pollet@icmcb-bordeaux.cnrs.fr.


### Notes

The authors declare no competing financial interest.

## ACKNOWLEDGMENTS


The authors would like to thank Dr. Ina Bucur (INCEMC), Mrs. Sonia Gomez (ICMCB), and Mr. Sebastien Fourcade (ICMCB) for their assistance during HT-XRPD, HRSEM measurements, and annealing experiments. S.R.P., M.M., A.V., and M.P. gratefully acknowledge financial support from European Community's Marie Curie Initial Training Network (ITN) Seventh Framework Programme - *SOPRANO* FP7/2007-2013 under Grant Agreement No. 214040. A.A. gratefully acknowledges financial support from European Community's Marie Curie Incoming International Fellowship (IIF) Seventh Framework Programme - *EPREXINA* FP7/2007-2013 under Grant Agreement No. 255662.


## REFERENCES


(1) Theobald, F. *J. Less-Common Met.* **1977**, *53*, 55.
(2) Kosuze, K. *J. Phys. Chem. Solids* **1967**, *28*, 1613.
(3) McWhan, D. B. *Phys. Rev. B* **1974**, *10*, 490.
(4) Andersson, G. *Acta Chem. Scand.* **1954**, *8*, 1599.
(5) Chamberland, B. L. *J. Solid State Chem.* **1973**, *7*, 377.
(6) Oka, Y.; Sato, S.; Yao, T.; Yamamoto, N. *J. Solid State Chem.* **1998**, *598*, 594.
(7) Theobald, F.; Cabala, R.; Bernard, J. *J. Solid State Chem.* **1976**, *438*, 431.
(8) Liu, L.; Cao, F.; Yao, T.; Xu, Y.; Zhou, M.; Qu, B.; Pan, B.; Wu, C.; Wei, S.; Xie, Y. *New J. Chem.* **2012**, *36*, 619.
(9) Wang, Y.; Zhang, Z.; Zhu, Y.; Li, Z.; Vajtai, R.; Ci, L.; Ajayan, P. M. *ACS Nano* **2008**, *2*, 1492.
(10) Wu, C.; Hu, Z.; Wang, W.; Zhang, M.; Yang, J. *Chem. Commun.* **2008**, 3891.
(11) Gui, Z.; Fan, R.; Chen, X. H.; Wu, Y. C. *J. Solid State Chem.* **2001**, *157*, 250.
(12) Gao, Y.; Bai, L.; Li, W.; Luo, H.; Jin, P. *J. Ceram. Soc. Jpn.* **2008**, *116*, 395.
(13) Menezes, W. G.; Reis, D. M.; Benedetti, T. M.; Oliveira, M. M.; Soares, J. F.; Torresi, R. M.; Zarbin, A. J. G. *J. Colloid Interface Sci.* **2009**, *337*, 586.
(14) Li, G.-c.; Pang, S.-p.; Wang, Z.-b.; Peng, H.-r.; Zhang, Z.-k. *Eur. J. Inorg. Chem.* **2005**, *2005*, 2060.
(15) Wu, C.; Dai, J.; Zhang, X.; Yang, J.; Xie, Y. *J. Am. Chem. Soc.* **2009**, *131*, 7218.
(16) Wu, C.; Feng, F.; Feng, J.; Dai, J.; Yang, J.; Xie, Y. *J. Phys. Chem. C* **2011**, *115*, 791.
(17) Li, W.; Dahn, J. R.; Wainwright, D. S. *Science* **1994**, *264*, 1115.
(18) Tsang, C.; Manthiram, A. *J. Electrochem. Soc.* **1997**, *144*, 520.
(19) Gui, Z.; Fan, R.; Mo, W. Q.; Chen, X. H.; Yang, L.; Zhang, S. Y.; Hu, Y.; Wang, Z. Z.; Fan, W. C. *Chem. Mater.* **2002**, *14*, 5053.
(20) Baudrin, E.; Sudant, G.; Larcher, D.; Dunn, B.; Tarascon, J.-M. *Chem. Mater.* **2006**, *18*, 4369.
(21) Wang, Y.; Takahashi, K.; Shang, H.; Cao, G. *J. Phys. Chem. B* **2005**, *109*, 3085.
(22) Sediri, F.; Gharbi, N. *J. Phys. Chem. Solids* **2007**, *68*, 1821.
(23) Li, X.; Chen, X.; Han, C.; Shi, C. *J. Cryst. Growth* **2007**, *309*, 43.
(24) Armstrong, G.; Canales, J.; Armstrong, A. R.; Bruce, P. *J. Power Sources* **2008**, *178*, 723.
(25) Kong, L. F.; Liu, Z. P.; Shao, M. W.; Xie, Q.; Yu, W. C.; Qian, Y. T. *J. Solid State Chem.* **2004**, *177*, 690.
(26) Liu, J.; Li, Q.; Wang, T.; Yu, D.; Li, Y. *Angew. Chem., Int. Ed.* **2004**, *43*, 5048.
(27) Oka, Y.; Yao, T.; Yamamoto, N. *J. Mater. Chem.* **1991**, *1*, 815.
(28) Li, G.; Chao, K.; Zhang, C.; Zhang, Q.; Peng, H.; Chen, K. *Inorg. Chem.* **2009**, *48*, 1168.
(29) Deschanvres. *C. R. Hebd. Seances Acad. Sci.* **1965**, *261*, 31.
(30) Rodríguez-Carvajal, J. *Phys. B* **1993**, *192*, 55.
(31) Valmalette, J.; Gavarri, J. *Mater. Sci. Eng., B* **1998**, *54*, 168.
(32) Sediri, F.; Gharbi, N. *Mater. Sci. Eng., B* **2007**, *139*, 114.
(33) Subba Reddy, C. V.; Walker, E. H.; Wicker, S.; Williams, Q. L.; Kalluru, R. R. *Curr. Appl Phys.* **2009**, *9*, 1195.
(34) Pavasupree, S.; Suzuki, Y.; Kitiyanan, A. *J. Solid State Chem.* **2005**, *178*, 2152.
(35) Leroux, Ch.; Nihoulm, G.; Van Tendeloo, G. *Phys. Rev. B* **1998**, *57*, 5111.